UNIVERSITY OF OSLO
Department of Geosciences
MetOs section

Assessing the relative dispersion of pairs of particles released in turbulent flows.

Master thesis in Geosciences
Meteorology and oceanography

Stine I. Mikalsen

25th June 2009

Abstract

Relative dispersion concerns the statistical calculations of pairs of particles released in flows. This is directly relevant to the dispersal of pollutants, whether in the form of a pollutant suddenly being discharged into the atmosphere, or an oil slick accidentally spilled into the ocean, as the mean drift and the spread can be derived from the calculations. Relative dispersion has additional value, due to the link to the energy spectrum of the underlying flow in which the particles are released, so that the behaviour of the particle trajectories can be used to infer characteristics about the flow. Two model data sets, each corresponding to an individual range of the energy spectrum: the energy cascade range (c–tank) and the enstropy cascade range (d–tank), together with one atmospheric observation data set from the EOLE balloon experiment, and one ocean surface observation data set from the SCULP experiment, have been examined in light of these relations. Two different statistical measures have been calculated: the relative dispersion and the diffusivity of pairs of particles in order to investigate which of the energy ranges the underlying turbulence for each of the data sets exhibit. The model data sets both show a dispersion growth in agreement with the predetermined wavelength intervals forced; the relative dispersion for c–tank has a dependency on time cubed, and the diffusivity has a dependency of distance in the 4/3 power, both results corresponding to the $\kappa^{\frac{-5}{3}}$ spectrum; the relative dispersion for d-tank has an exponential dispersion growth and the diffusivity has a dependency of distance squared, corresponding to the κ^{-3} spectrum. The SCULP drifter data presents an exponential growth for the first 10–11 days, followed by a power law growth of $t^{2.2}$ for the longest times. The EOLE balloon data, however, are the subject of discussion; the results calculated here show either an exponential growth or a power law growth for the relative dispersion, depending on which balloon pairs are taken into consideration.

Acknowledgements

First and foremost, I would like to thank my supervisor, professor Joseph H. LaCasce, for a most interesting task and for providing me with both the model and observational data needed for the calculations. I can honestly say that I found it quite hard to wrap my brain around all these unfamiliar theories and relations in the beginning, so, thank you for your instructive guidance and for patiently answering my questions throughout the working process, and especially during the last weeks prior to handing in my thesis.

I would also like to thank all of my friends and fellow students for good humouring me and helping me keep going whenever my faith in my own abilities was set to the test. And especially – Ann Kristin: thank you for answering all of my occasionally odd and stupid, but always well formed (ha ha) questions regarding Matlab; Karianne and Nina: thank you ever so much for proofreading parts of my thesis, even up until the last minute.

Last but not least I would like to thank my family for always supporting me and asking questions about my studies, even though I honestly doubt they understand what I am talking about when I rattle on about my thesis. Still, thank you for everything!

Oslo, June 2009

Stine Mikalsen

Contents

Chapter 1

Introduction

The world's oceans and atmosphere are constantly on the move. The currents flow in complex patterns and are affected by many forces. One of the oldest methods for studying the circulation is to release something into the ocean or atmosphere and let the flow carry it wherever it may go. Using such oceanic devices known as drifters or floats, scientists have increased the understanding of the complexities of global ocean currents, and, in turn, the many systems that they influence. For the atmosphere meteorological balloons can provide similar understanding of the atmospheric circulation.

The data garnered from these devices allow scientists to design models of climate and weather patterns, such as El Niño and hurricanes, as well as predict where pollutants, such as oil or sewage, will drift if they are dumped or accidentally spilled into the ocean. In the event of toxic substances or pollutants being discharged into the atmosphere or ocean e.g. through the emission of sulphur dioxide (SO_2) from volcanic eruptions or oil spill from ships, the most important responsibilities for the authorities in charge are to, if possible, limit the damages caused by the pollutant, and to warn the population in the case of a potential hazard. The spread of such a pollutant in the form of a "cloud of tracer" (collection of particles), is caused by the turbulent flow features of the total stream, and the ability to cause dispersion is determined by the energy spectrum of the underlying turbulence. An in–depth knowledge of the dynamics causing the stirring, and the various outcomes depending on which energy regime the turbulence occupies, is therefore of vital importance, as this can make us better suited for controlling and predicting the movement and spread of a cloud of tracer.

The mean drift of such a cloud of tracer, whether it is a pollutant cloud in the atmosphere or an oil slick in the ocean, is reflected through the displacement of the centre of mass. Of equal importance is the cloud dispersion, i.e. how the particles spread out about the centre of mass, which can be measured by the variance (mean square) of the displacements of the individual particles that constitute the cloud (also referred to as the relative dispersion) (LaCasce, 2008). As will be shown in chapter 2, the relative dispersion is

related to the statistics of pairs of particles released in flows (Lagrangian trajectories), in addition to being linked to the energy spectrum of the flow, so that several measuring methods can be combined when studying the dispersal of a cloud of tracer in the attempt to gain a better understanding of the underlying eddy turbulence and the pertaining energy spectrum.

Scientists have ever since Taylor (1915) first recognized eddy turbulence in the atmosphere, studied the subject of both atmospheric and oceanic dispersion with various results. At first, the difficulties regarding sampling and monitoring either fluid limited the studies both in terms of the size of the sampling area and in number of observations made.

Observations of kites by eye (Taylor, 1915) or studies of smoke plumes in the atmosphere (Richardson, 1926) were used to form the basis for calculations. Even though the methods may seem simple, the results implied eye-opening discoveries of eddy turbulence, the energy spectrum and the pertaining dispersions, and consequently the prevailing doctrines were altered.

Richardson's (1926) extensive work examined the dispersion of smoke plumes in the atmosphere with regard to Fick's equation for standard molecular diffusion

$$\frac{dv}{dt} = K\frac{d^2v}{dt^2} \tag{1.1}$$

where v can be any kind of variable, e.g. density, velocity components, a tracer, and where K is the constant diffusion coefficient. Richardson concluded that Fick's law was quite unsuitable for this purpose, and instead found a dependency of length scales in the $4/3$ power of the diffusivity, at present known as the Richardson's law for the dependence of turbulence diffusivity on the relative particle separation.

$$K(D) \propto D^{\frac{-4}{3}} \tag{1.2}$$

where D is the distance between particles.

In an attempt to transfer this theory to the ocean, Richardson and Stommel (1948) repeatedly studied the relative dispersion of two floating pieces of parsnip set out from Blairmore Pier in Scotland, and they found most interestingly that Richardson's law was a rather good fit also for the diffusivity at the ocean surface.

With the progress of radar came the development of acoustically tracked instruments, and this yielded the possibility for a closer study of the ocean than earlier, e.g. with the use of the Swallow float (Swallow, 1955) which immediately implied huge consequences for the perception of the ocean at that time. In fact, the prevailing theory was of the subsurface currents to be

decreasing towards the bottom and in general have quite small velocities at great depths, but a study by Swallow and Worthington (1961) that indicated a southward undercurrent of the Gulf stream with velocities of more than 15 cm s^{-1} demolished this theory and cleared the path for Stommel's (Stommel and Arons, 1960) theory of a deep thermohaline circulation.

The further development regarding both floats and drifters is well accounted for by Davis (1991), e.g., the discovery of the SOFAR (Sound Fixing And Ranging) channel, in which sound is refracted and ultimately spread in a cylindrical pattern, led to the opportunity of long-range tracking and therefore many new studies of Lagrangian data in the ocean. As a consequence of the effort to improve the instrument itself, but also due to an attempt to economize the whole process of tracking and sampling, the development of RAFOS floats (SOFAR spelled backwards; Rossby et al. (1986)) resulted in reducing the size of the float. Then the introduction of the Autonomous LAgrangian Current Explorer floats (ALACE) and the Profiling ALACE floats (PALACE), which both are tracked by satellites (Davis et al., 1992), consequently broadened the sampling region and reduced the costs of experiments.

The satellite era also paved the way for extensive tracking of balloons in the atmosphere and resulted in a huge breakthrough in regard to monitoring, thus several experiments were conducted. The EOLE experiment during the 1970s (Morel and Bandeen, 1973), and the TWERLE (Tropical Wind, Energy conversion and Reference Level Experiment; Julian et al., 1977) in the 1980s, which observed balloons in the Southern Hemisphere at the 200 mb-level and the 150 mb-level respectively, provided Lagrangian data which even up till this date are used as basis for numerous studies.

The various studies throughout the history of "the science of eddy turbulence" have resulted first of all, as noted above, with the replacement of Fick's law when it comes to calculating the diffusivity due to eddy turbulence. It is now commonly accepted that there exists a scale dependency of the diffusivity of pairs of particles. However, what shape this dependency takes, i.e. what range of the energy spectrum the dependency lies within, is debated.

Observations of the dispersal of particles in both the atmosphere and ocean must therefore be studied with regard to the underlying turbulence to improve the knowledge of how different energy spectra imply different dispersal patterns. Such observations should then be compared to model experiments so that we can deduce how particles spread given various initial conditions and turbulent flows, hence improving the skill of predicting the spread of a cloud of tracer. It is also of interest to see which statistical measure is the most robust for calculating the dispersal. Two distinct model data sets will be studied in this theses, each corresponding to a predetermined wavelength interval for which the energy spectrum of the model is forced, in order to

distinguish between the two dispersal species of question in this study.

Of special interest in regard to this thesis are the previous studies of Lagrangian data from some of the abovementioned experiments that focus on statistical calculations of the spread of pairs of particles and the pertaining energy spectrum of the underlying turbulence. Morel and Larcheveque (1974) and Lacorata et al. (2004), both made use of the EOLE data, but as will be shown in section 4.3, they did not arrive at the same conclusion, likely due to the different measures used. In this thesis, two different measures, the relative dispersion and the diffusivity, will be examined, and then compared with the results from both previous studies, trying to make the conclusions regarding the relative dispersion and the underlying energy spectra of the turbulent flow somewhat clearer.

In addition to the balloon trajectories, this study will make calculations based on data from the SCULP (Surface CUrrent and Lagrangian drifter Program) experiment, which consist of several deployments of drifters into the Gulf of Mexico during the 1990s (Ohlmann and Niiler, 2005). The SCULP data have been studied by LaCasce and Ohlmann (2003) with focus on the relative motion of pairs of surface drifters. A subset of the SCULP data will be studied in this thesis, and compared to the results of LaCasce and Ohlmann (2003).

The structure of this thesis is as follows: Chapter 2 starts with a brief description of the development of sampling instruments, followed by a presentation of the underlying theory associated with relative dispersion of Lagrangian particles, both for single particle statistics and multiple particles statistics. Chapter 3 gives a description of the data sets used in this thesis. The results exhibited by the various statistical calculations of these data are presented in chapter 4, whereupon a summary and some concluding remarks are given in chapter 5.

Chapter 2

Theory

This chapter leads off with a brief overview of the various instruments used to sample Lagrangian data in the atmosphere and ocean. Some general consepts of the relationship between the dispersal of a cloud of tracer and the statistics from Lagrangian data are then accounted for, followed by a more thorough description of the single and multiple particle statistics forming the basis for the calculations in this thesis. The derivations and calculations in this chapter are given in accordance with LaCasce (2008).

2.1 Instruments

Lagrangian instruments in general have the advantage of being free-drifting, and can therefore monitor large areas in both the atmosphere and ocean on their own. The fact that Lagrangian instuments usually end up following very complex paths makes the methods of analysis somewhat different than for data from Eulerian observation instruments. The most commonly used instruments are floats and drifter in the ocean, and balloons in the atmosphere.

Instruments for observing the ocean in regard to Lagrangian measures, can be devided into two categories: drifters, which follow surface currents, and floats, which follow subsurface currents (LaCasce, 2008).

Drifters consist of a subsurface device, a drogue in general in the shape of a kite, which is kept at a constant depth usually between 5–50 meters, and attached to a surface transmitter, which for the majority of drifters, is tracked with the Argos satellite system. Recent drifter models can be tracked by GPS if used for near-shore observations. Figure 2.1 shows the CODE drogued drifter (Davis, 1985), as an example. This CODE drifter has a kite–like drogue, and both a surface– and a subsurface float, in addition to an antenna and a transmitter package in charge of monitoring.

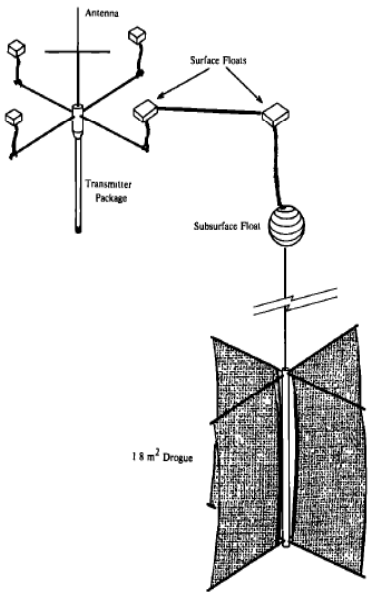

Figure 2.1: The CODE drogued drifter. The drogue assembly has a negative buoyancy of 2.8 kg, the subsurface float provides 2.6 kg buoyancy, and the area of the drogue is 1.8 m^2. Figure from Davis (1985), page 4742.

For monitoring subsurface currents, various types of floats are used. Floats are constructed to sink to a predetermined depth where they follow the current in question. Such floats have ballasting and a certain compressibility to maintain their chosen depth. However, floats can also be modified to follow density surfaces, so that they behave even more like a Lagrangian particle than constant-depth floats, which in fact are just "quasi–Lagrangian". Due to the ocean's opaqueness to acoustic waves, floats can not be tracked by satellites, but monitoring by the emittance and recording of low frequency sound pulses are the most common, used for Swallow floats (Swallow, 1955), SOFAR floats (Rossby and Webb, 1970) and the reverse RAFOS floats (Rossby et al., 1986). The latest development is the ALACE (Davis et al., 1992), and PALACE floats, which keeps at a constant depth only to rise to the surface at fixed intervals to be located by satellite, the latter also measuring the density while it rises to the surface, hence the name "Profiling ALACE".

Before satellites made a huge impact on how the atmosphere is monitored, by-eye observations of smoke plumes and kites were some of the bases for atmospheric studies. However, being able to accurately monitor atmospheric variables by satellite soon made this the preferable method. For decades now, scientists have launched balloons into the atmosphere to measure and track weather patterns, with very encouraging results. Figure 2.2 shows an example of a balloon used in the TWERLE experiment. The balloon carries instru-

ments for measuring different variables in the atmosphere, e.g. temperature (not shown in the picture), pressure and height, whilst other instruments are for enabling tracking. Some balloons of today are even releasing small driftsondes that transmits temperature, wind and pressure data to a satellite as it drifts to earth.

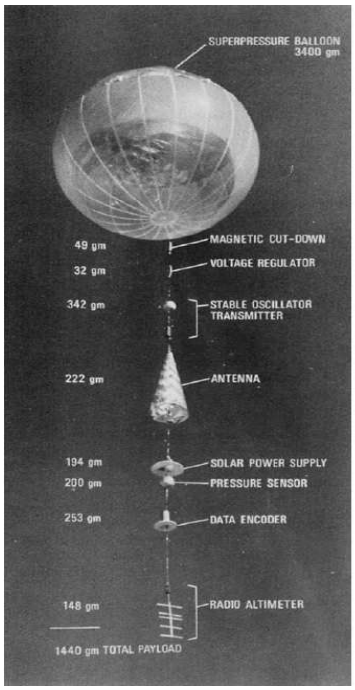

Figure 2.2: Schematic photo of a TWERLE balloon when at floating altitude. The TWERLE balloons were launched into the atmosphere at the 150–mb level during the 1980s. The balloons carried both measuring and tracking instruments. Figure from Jullian et al. (1977), page 937.

Hence sampling in the atmosphere nowadays is simplified by the use of satellites for tracking, and Lagrangian observations together with the possibilities to obtain vertical profiles from remote sensing techniques, has resulted in the atmosphere being very well monitored over the years. In comparison, the ocean is still in need of vast investigations to unfold the knowledge still not accounted for.

2.2 General concepts of Lagrangian statistics

Statistics of Lagrangian data imply averaging the positions and/ or the velocities of the particles observed. The results yield different statistical measures that concern either single or multiple particle statistics, and in order to describe the dispersal of a tracer in the atmosphere or ocean, both such are

needed. As noted in chapter 1, the displacement of the centre of mass of a cloud of tracer is described by the mean drift, here in the x-direction

$$M_x(t) = \frac{1}{N}\sum_{i=1}^{N}[x_i(t) - x_i(0)] \tag{2.1}$$

where N is number of particles in the cloud and $x_i(0)$ and $x_i(t)$ the initial position and the position at time t = t for each individual particle, respectively. The mean drift is the average for the displacement of each individual trajectory that consitutes the cloud, i.e. it is a single particle measure, and it is the first moment of the displacements.

The second-order moment

$$D_x(t) = \frac{1}{N-1}\sum_{i=1}^{N}[x_i(t) - x_i(0) - M_x(t)]^2 \tag{2.2}$$

i.e. the variance (mean square) of the displacements, yields the spread of the particles around the centre of mass. This is also referred to as the dispersion, and it can be expanded so that it is valid for N number of particles, i.e. the sum over all particle pairs

$$D_x(t) = \frac{1}{2N(N-1)}\sum_{i\neq j}[x_i(t) - x_j(t)]^2 \tag{2.3}$$

Thus the dispersion of the cloud (eq. 2.3), is proportional to the mean square pair separation (for eq. 2.3: the sum of the squared separations for all N particles of the cloud). This is a helpful correlation which links the concentration statistics of a cloud to the general two particle statistics, and as a consequence, the cloud dispersion can be determined from statistics obtained from repeatedly releasing pairs of particles into a flow instead of the observation or modelling of the whole cloud, which indeed contains much more than just a number of particle pairs, even if iterative pair observations are needed to have a statistically significant measure.

The favourable potential for the dispersion to calculate the size of the cloud, is quite impaired by the fact that the dispersion on the other hand portrays the cloud's distribution in space rather poorly.

To gain a better understanding of the displacement, the probability density function (PDF) of the displacements is introduced. The PDF is generated by binning the particles by distinct displacement distances from the centre of mass, and this yields a histogram showing the number of particles for each of the distance bins, providing a clearer picture of the displacement around the centre of mass. In addition to providing a figurative measure of the displacement, the PDF can generate all the moments, e.g. the mean,

dispersion, and yet another moment called the kurtosis. While the dispersion measures the width of the PDF, the kurtosis measures the "peakedness" of the PDF. A Gussian shaped PDF (frequent modestly-sized deviations) has a kurtosis of 3, as apposed to a higher kurtosis which implies that more of the variance is due to infrequent extreme deviations, where few observations are far from the mean, and the majority is conentrated on or around the mean. The kurtosis is the fourth-order moment of the displacement:

$$ku(x) \equiv \frac{\sum_i (x_i - M_x)^4}{[\sum_i (x_i - M_x)^2]^2} \tag{2.4}$$

These abovementioned measures will be the basis for the analyses throughout this thesis. All the moments (mean, dispersion and kurtosis) can be derived for either displacements or velocities to yield different measures. The single particle calculations are presented first, followed by multiple particles.

2.3 Single particle statistics

For a single particle, a PDF for the displacement from $x = x_0$ at $t = t_0$, to $x = x_1$ at $t = t_1$, can be defined

$$Q(x_1, t_1 \mid x_0, t_0) \tag{2.5}$$

If a cloud of particles is considered, the PDF is re-written

$$P(x_1, t_1) = \int P(x_0, t_0) Q(x_1, t_1 \mid x_0, t_0) dx_0 \tag{2.6}$$

thus integrating over all of the initial posistions consituting the cloud. For a statistically homogeneous and stationary flow, the PDF ultimately yields

$$Q(x_1, t_1 \mid x_0, t_0) = Q(x_1 - x_0, t_1 - t_0) \equiv Q(X, t) \tag{2.7}$$

This PDF is used when calculating all the statistical moments. The mean displacement (first moment)

$$\overline{X} = \int X Q(X, t) dX \tag{2.8}$$

the single particle dispersion (second moment)

$$\overline{X^2}(t) = \int X^2 Q(X, t) dX \tag{2.9}$$

and the absolute diffusivity (the time derivative of the single particle dispersion)

$$\kappa(t) \equiv \frac{1}{2} \frac{d}{dt} \overline{X^2} = \overline{X(t) u(t)} = \int_0^t \overline{u(X, t) u(X, \tau)} d\tau \tag{2.10}$$

which means that the diffusivity is the integral of the velocity autocorrelation.

2.4 Multiple particle statistics

As noted earlier, (chapter 1), the relative disperson equals the mean square distance between pairs of particles, and it describes how a cloud of tracer spreads about its centre of mass. In addition it gives the sensitivity to the trajectory's initial position. The early and late development in time of the dispersion is quite the same as for the absolute dispersion (section 2.2). Of major interest though is how the relative dispersion evolves at inter–mediate time scales, as this is strongly influenced by the Eulerian mean and hence, the underlying energy spectrum of the flow which is of great interest in turbulence studies.

The discovery of the fact that the dispersion did not obey Fick's equation, urged the need for studies of turbulent flows, and it was soon stated that the turbulent mixing in the planetary boundary layer could explain the dispersion there and that the diffusivity has a scale dependency.

Still in accordance with the calculations by LaCasce (2008), the theory of multiple particle statistics now follow.

As for the single particle statistics, a PDF for the particle separations can be constructed:

$$q(y,t \mid y_0,t_0) = \int L(x,y,t \mid x_0,y_0,t_0)dx_0 \tag{2.11}$$

where the integration is over the initial positions, x_0. This PDF can be further developed to a PDF of the event of observing a particular separation between pairs

$$p(y,t) = \int p(y_0,t_0)q(y,t \mid y_0,t_0)dy_0 \tag{2.12}$$

from which the moments can be derived, in a similar manner as for the single particle statistics, e.g. the second order moment (the relative dispersion)

$$\overline{y^2}(t) = \int y^2 p(y,t)dy \tag{2.13}$$

and the relative diffusivity (the time derivative of the relative dispersion)

$$\kappa \equiv \frac{1}{2}\frac{d}{dt}\overline{y^2} = \overline{yv} = \overline{y_0 v} + \int_{t_0}^{t} \overline{v(t)v(\tau)}d\tau \tag{2.14}$$

As seen in section 2.1.3, where the absolute diffusivity is derived from the velocity autocorrelation, the relative diffusivity for pairs of particles is now derived from the two particle velocity cross–correlation ($v(t)v(\tau)$). Also, in the same manner as for single particle statistics, the relative dispersion for pairs of particles behaves like the absolute dispersion at the smallest and largest scales, and again the interest lies in the intermediate scales, in which

the dispersion depends on the flow. Assuming the flow is homogeneous, and using the first Bessel function when calculating the Eulerian wavenumber spectrum, the relative dispersion for intermediate scales is

$$\overline{v(y)^2} \propto y^{\alpha-1} \tag{2.15}$$

and the corresponding diffusivity

$$K = \frac{1}{2}\frac{d}{dt}\overline{y^2} \propto y^{\frac{\alpha+1}{2}} \tag{2.16}$$

This yields a separation dependency of the diffusivity, and this is reflected by the slope of the energy spectrum. For this range, the dispersion is referred to as "local", due to the dominating eddies having the same scale as the separation between the pair of particles.

As α has values between 1–3 for intermediate scales, the diffusivity will be proportional to the distance in a 4/3 power for $\alpha = 3$, i.e. Richardson's law.

For $\alpha \geqslant 3$ (steep wavenumber spectra), the relative dispersion will be dominated by eddies larger than the separation between pairs, i.e. the dispersion is "non–local", and can be expressed as

$$\overline{v(y)^2} \approx \frac{1}{2}y^2 \int k^2 E(k) k = c_1 \Omega y^2 \tag{2.17}$$

where c_1 is a integration constant, and Ω is the total enstrophy (the integrated square velocity). The diffusivity is

$$K = \frac{1}{2}\frac{d}{dt}\overline{y^2} = c_2 T^{-1}\overline{y^2} \tag{2.18}$$

which corresponds to an exponential growth of the separation of pairs of particles, also referred to as "Lagrangian chaos".

2.4.1 Turbulent dispersion and energy spectra

The turbulence in the boundary layers of both the atmosphere and ocean can be used as an example of the relative dispersion that occurs in these layers. Due to the vertical motion being effective here, the turbulence is three dimensional and the energy is being transported towards larger scales, i.e. the spectrum has a $\kappa^{\frac{-5}{3}}$ dependency. Further away from the planetary and surface boundary layers, the vertical velocity is reduced, thus yielding a two dimensional turbulence. The $\kappa^{\frac{-5}{3}}$ dependency is recognized here as well, leading to a relative dispersion for the energy inertial range (energy cascade range)

$$\overline{y^2} \propto \epsilon t^3 \tag{2.19}$$

with corresponding diffusivity

$$K \propto \epsilon^{\frac{1}{3}} y^{\frac{4}{3}} \tag{2.20}$$

where ϵ is the constant energy dissipation rate for energy transport from small scales towards larger scales. Again, the diffusivity coincides with Richardson's law of the 4/3 dependency of scales.

Two–dimensional turbulence exhibits another energy inertial range though, the enstrophy cascade range, in which enstrophy is transported from slightly large scales towards smaller scales before it is dissipated. In this spectrum range, the relative dispersion has a exponential growth:

$$\overline{y^2} \propto e^{c_3 \eta^{\frac{1}{3}} t} \tag{2.21}$$

and the diffusivity has a dependency of distance squared:

$$K \propto \overline{y^2} \tag{2.22}$$

where η is the enstrophy dissipation rate.

Thus two–dimensional turbulence depends on the distinct energy cascade for which the pair of particles experiences.

2.4.2 Diffusivity as a measure

The diffusivity as a measure concerns calculating the mean over the distances instead of time as for the relative dispersion, and is a more robust measure for the development of the displacement distribution. This is because pairs of particles can present very different pair separations from time to time, and when sampling all the particle pair separations within a "cloud of tracer" at a fixed time, the mean will be affected of possibly statistical outliers with "too large" separations compared to the majority of the particle pairs within the "time bin". When calculating the diffusivity, i.e. a measure that averages over distances, at fixed distance bins, no such outliers exist, hence the diffusivity gives a more accurate result of the dispersion.

Chapter 3

Data

The data used in this thesis consist of two sets of model data and two sets of observational data. The model data are derived from a numerical experiment model where, with the purpose of this thesis, the forcing term in the equation solved by the model is defined to reflect two different energy spectra, and hence two distinct particle trajectory developments. In addition, one atmospheric observation data set (EOLE) and one ocean surface observation data set (SCULP) are studied. This chapter gives an overview of the data sets and their basics. The results derived from the statistical calculations of the data sets will be presented later, in chapter 4, where also comparisons between calculations in this study and previous work will be done.

3.1 Model data

Two sets of model data are presented in this study; both sets originate from a simplified and modified version of the model used in LaCasce and Brink (2000). The version of the model used in this thesis employs one horizontal, either atmospheric or oceanic layer (thus the model can numerically produce particle trajectories for either fluid), and a flat bottom confined to a domain of 2π x 2π. The model is double-periodically, which implies that whenever energy passes through one side of the domain , the same energy re-enters the opposite side simultaneously. The dynamic equations governing the flow are quasi-geostrophic, and the planetary gradient is set to be zero, i.e. $\beta = 0$. The use of the quasi-geostrophic equations makes the computations more efficient than with the primitive equations. For time stepping, a standard leapfrog scheme is used, with an Euler step every 50th step to suppress computational errors.

The model solves the equation

$$\frac{d}{dt}\nabla^2\psi + u\frac{d}{dx}\nabla^2\psi + v\frac{d}{dy}\nabla^2\psi = F - D \tag{3.1}$$

where ψ is the stream function, and u,v the zonal and meridional velocities respectively. Running the model ultimately yields the trajectories of the individual particles deployed into the turbulent flow. The diffusive term, D, is

the Ekman friction. The forcing term, F, is a stochastic forcing function, that for each time step randomly alters the turbulent eddies, and consequently the energy spectrum and the dispersion of the particles as well. The non-linear terms (terms 2 and 3 on the left side) are responsible for the interaction between the different energy modes in the model, and thus the dissipation of energy between modes.

As the model starts up, energy is added to the forcing term in a predetermined wave number interval depending on which range of the energy spectrum being examined. Initially, some adjustment is needed for the model to reach steady state between the forcing and diffusion terms. Figure 3.1 shows the development of the total energy (KE) for d-tank model data set as a function of time. The total energy increases rapidly as the energy is added in the wavelength interval forced at time t = 0. As soon as the total energy within the domain reaches statistically steady state (approximately at time t = 12), the particles are deployed, and their positions are recorded in time.

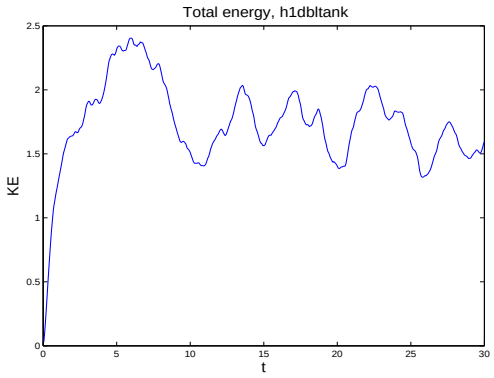

Figure 3.1: The development of the total energy (KE) for the d-tank model data set as a function of time after deployment.

This thesis employs two distinct model data sets, hereafter named c-tank and d-tank. For c-tank data set, the addition to the forcing term is in the wave number interval, $L = [\frac{2\pi}{60}, \frac{2\pi}{50}]$, which implies forcing at small scales, resulting in an energy cascade to larger scales, while on the other hand, for the d-tank data set, the forcing is added in the wave number interval, $L = [\frac{2\pi}{5}, \frac{2\pi}{1}]$, i.e. at large scales, ultimately transporting enstrophy towards the smaller scales over the range of wavelengths resolved by the model. Figure 3.2 shows particle trajectories for 6 randomly selected particles deployed in a) d-tank, and b) c-tank. The initial positions for all the particles deployed are in the interval $x = y = [3.1 - 3.2]$ for both data sets. The trajectories display very different developments, due to the forcing of the underlying turbulence being added at different wavelengths. Note also the difference in values on the axes. The particles in c-tank are spread much further from the initial positions than the particles in d-tank, implying that the underlying turbulence in c-tank in general results in larger dispersal of the particles.

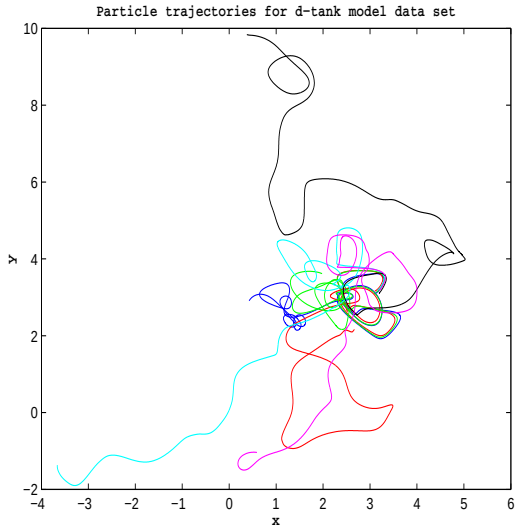

(a)

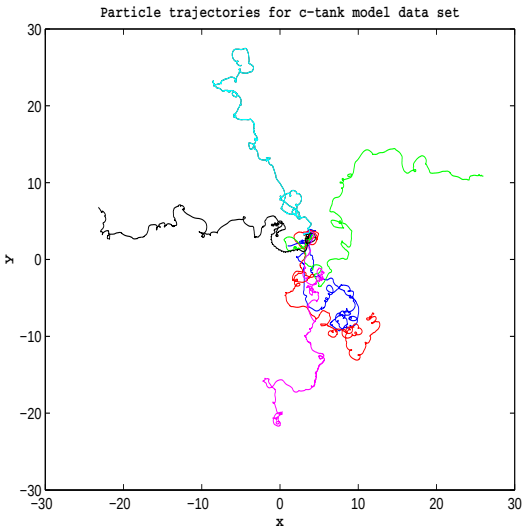

(b)

Figure 3.2: Particle trajectories for 6 randomly selected particles deployed in a) d-tank, and b) c-tank. Note the different scales of the axes! In general, the particles from the c-tank data set are spread further from their initial positions than the particles from d-tank data set.

3.2 Observation data

3.2.1 SCULP data

The oceanic observation data used in this study were obtained from the Surface CUrrent and Lagrangian drifter Program, SCULP, which consists of 3 individual routine drifter deployments, hereafter named SCULP-I, -II and -III (Ohlmann and Niiler, 2005). Each set of deployments was carried out during different periods from October 1993 to July 1996. The data provide observations of individual trajectories from surface drifters deployed in various regions in the Gulf of Mexico.

The drifters were designed similarly to the drifters used in the Coastal Ocean Dynamics Experiment (CODE; (Davis, 1985). Four rectangular panels 50 cm wide by 90 cm tall were assembled to a vertical tube 10 cm in diameter. The centre of the drifter was kept near 0.5 m depth by small surface floats attached to the drifters with flexible cords, as shown in Figure 2.1. The drifters were tracked by the Argos satellite locating system, and their positions were fixed within a 300 m-1000 m circle 5-7 times a day by Doppler ranging.

In the SCULP-I deployment, 409 drifters were set out on the Louisiana-Texas shelf from October 1993 through July 1994. The deployment occurred either from one of three oil producing platforms with weekly deployments for 44 weeks, or periodically from aircraft in a predetermined set of 15 stations. The aircraft-deployed stations were seeded with a new drifter only when no other drifter was localized within 5 km of the station the day before the deployment flight. All in all the SCULP-II deployments covered a 125 km square sampling grid, and a total of 374 drifters were traceable for a minimum of two days with a half life time of 56 days.

The SCULP-II deployment began in February 1996, and the drifters were set out from aircraft to 15 different stations within a 500 x 200 km grid on the Northwest Florida shelf. 11 new stations were added later on, and deployment of the whole 26-station set was carried out from April 1996 through February 1997. A total of 359 drifters were employed and 342 of them survived more than two days, with a half life time of 66 days. Figure 3.3 shows the trajectories of the SCULP–I and -II drifter pairs with initial separation, $r_0 \leq 1km$, for the first 25 days after deployment, as an example of trajectories.

The third set of drifter deployments, SCULP-III, was focused on a particular flow feature, i.e. the effect of gulf eddies on drifters across the shelf-rise. Two anticyclone eddies were identified; one over the shelf-rise south of Louisiana and one on the northwest Florida shelf-rise. Consequently 20 drifters were seeded twice in each of the two structures during April and July 1998. Of 80 drifters deployed, 67 gave trajectories of more than two days. As a consequence of a small number of drifter pairs and the fact that the SCULP-III

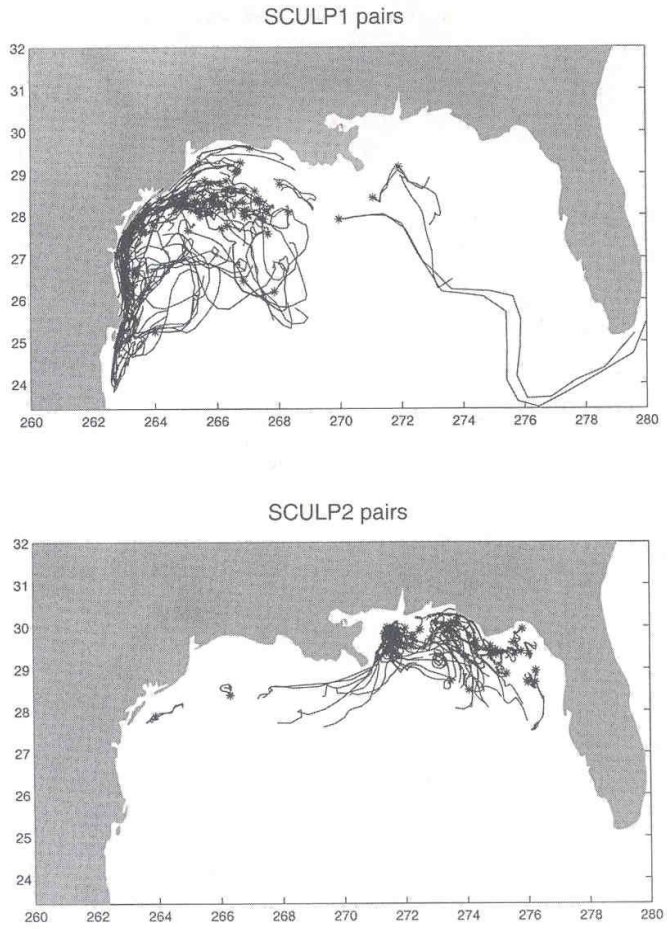

Figure 3.3: Trajectories of some of the SCULP drifters from SCULP–I (top) and -II (bottom) data set. Figure from LaCasce and Ohlmann (2003), page 289.

set focused on a particular flow feature, these trajectories are not included in the dataset used in this thesis.

3.2.2 EOLE data

The atmospheric observation data used in this study were obtained from the EOLE experiment which took place from August 1971 to July 1972 (Morel and Bandeen, 1973). A total of 480 constant-volume balloons were released from three different sites in Argentina to the 200 mb-level in the Southern Hemisphere. Figure 3.4 shows trajectories for three individual EOLE balloons. The balloons were tracked by the EOLE navigation and data collection satellite which was launched in 1971. Average lifetime of the balloons was 120 days. Large quantities of Lagrangian data (balloon trajectories) were generated from this experiment, which from then on formed the basis for numerous studies, both in Lagrangian and Eulerian perspectives. Morel and Desbois (1974) estimated the climatologically aspects of the general

circulation, and Desbois (1975) computed the planetary- and synoptic-scale kinetic energy space spectra on the basis of the horizontal displacements of EOLE balloons. Actually, the EOLE data remain to this day one of the most ample data sets with the purpose of studying quasi-Lagrangian particles and the properties of intermediate motion at the tropopause level (Lacorata et al., 2004).

Figure 3.4: Trajectories of three EOLE balloons, numbered 247, 249 and 250, released almost simultaneously from Mendoza, Argentina, on 20th September 1971. Figure from Morel and Bandeen (1973), page 301.

Several scientists have studied the data obtained from the EOLE experiment. One great advantage of such a large quantity of observations as in the EOLE experiment is that the statistics calculated from the data are statistically significant, thus more reliable. Morel and Larcheveque (1974)analyzed 12.239 individual estimates of the relative dispersion rate of balloon pairs provided by the EOLE experiment, and calculated the two particle relative dispersion obtained from the balloon trajectories.

Chapter 4

Results and discussion

The results from the statistical calculations of both model data sets and the EOLE and SCULP observations are presented in this chapter. First, the model results are examined, trying to validate the relative dispersion growth for each data set in accordance to its underlying turbulence, determined by the distinct wavelength interval in which the energy spectrum is forced. Preferably, the results will demonstrate two distinct growth regimes, thus providing a good standard of reference when studying the observational data.

Calculations of the data from the SCULP and EOLE experiments are then presented, first individually, along with some remarks on previous studies. Especially the EOLE data have led to some discrepancies among scientists.

4.1 Model results

4.1.1 C-tank

In the c-tank model data set, the forcing is added in the wavelength interval, $L = [\frac{2\pi}{60}, \frac{2\pi}{50}]$, which implies that the dispersion of pairs of particles is influenced by eddy turbulence in the energy cascade range of the energy spectrum for which the model is resolved. This entails energy being transported from small scales towards larger scales where it eventually is dissipated. The relative dispersion presumably has a dependency of time cubed ($\overline{D^2} \propto t^3$), and the diffusivity should follow Richardson's law and show a scale dependency in the 4/3 power ($K \propto D^{\frac{4}{3}}$), in order to verify the model set up for the particular forced wavelength interval chosen for the c-tank data set.

Figure 4.1 shows the zonal (x) and meridional (o) components of the relative dispersion of pairs of particles as a function of time after deployment. The straight line represents a t^3 power law growth, and is a rather good fit for t $= 3 \times 10^5 - 2 \times 10^6$. Note that the values on the x-axis in this figure are incorrect. This is a result of the plotting function in Matlab, and for this particular plot only – the agreement between the relative dispersion components

and the straight line is still correct. For longer times, the growth decreases, which is expected due to energy being dissipated here, thus impairing continuously cubed growth. The model is not unaffected by noise though: at time t = 2×10^5, a rather distinct discrepancy is shown, but this does not disrupt the general agreement to a t^3 power law growth for longer time scales.

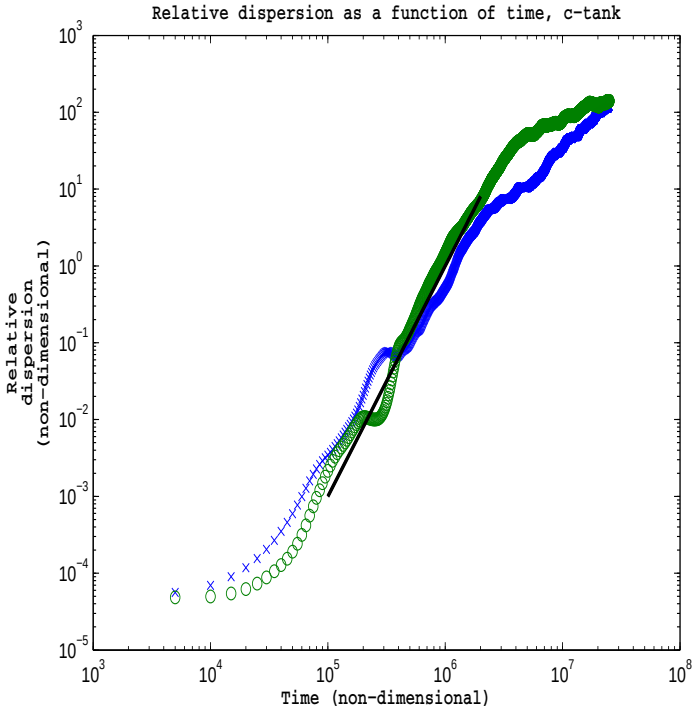

Figure 4.1: The zonal (x) and meridional (o) component of the relative dispersion as a function of time after deployment. The straight line represents a t^3 power law, which corresponds to a energy cascade range of the energy spectrum. Note that the values on the x-axis in this figure are incorrect. This is a result of the plotting function in Matlab only – the agreement between the relative dispersion components and the straight line is still correct.

However, as noted in section 2.5, the diffusivity usually is a more robust measure of the growth of the relative dispersion due to averaging over distance as opposed to time. Figure 4.2 shows the diffusivity for pairs of particles as a function of distance. The straight line represents a $D^{\frac{4}{3}}$ law, i.e. Richardson's law, and shows a quite good fit up to distances of D = 1. This result does not present an accurate agreement between particle separation growth and the $D^{\frac{4}{3}}$ law either, but for the use of the following comparisons with observational data in this study, the relative dispersion for c–tank is assumed to follow Richardson's law, which yields that the underlying turbulence is within the $\kappa^{\frac{-5}{3}}$ energy spectrum up to distance D = 1.

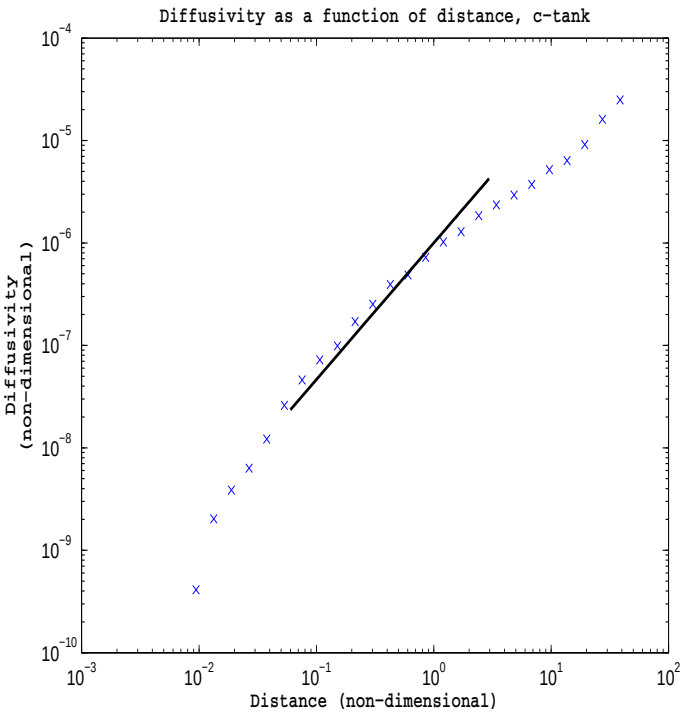

Figure 4.2: The diffusivity for c-tank model data set as a function of distance. The straight line represents the $D^{\frac{-4}{3}}$ law, which corresponds to the $\kappa^{\frac{-5}{3}}$ region of the energy spectrum.

4.1.2 D-tank

In the d-tank model data set, the forcing of the energy spectrum is added in the wavelength interval $L = [\frac{2\pi}{5}, \frac{2\pi}{1}]$, which implies that the dispersion of pairs of particles is influenced by the enstrophy cascade range of the energy spectrum for which the model is resolved. Hence the relative dispersion is presumed to experience an exponential growth in time ($\overline{y^2} \propto e^t$), and the diffusivity should show a dependency of distance squared ($K \propto \overline{D^2}$). The d-tank data set has a forcing that ensures the transport of enstrophy from large scales towards smaller scales, where it eventually is dissipated.

Figure 4.3 shows the zonal (x) and meridional (o) components of the relative dispersion of pairs of particles as a function of time after deployment. The straight line represents an exponential growth, i.e. the enstrophy cascade range of the spectrum. The relative dispersion displays a fairly poor fit to the exponential growth line, and the dispersion also exhibit a somewhat anisotropic behaviour (i.e. the zonal and meridional components differ).

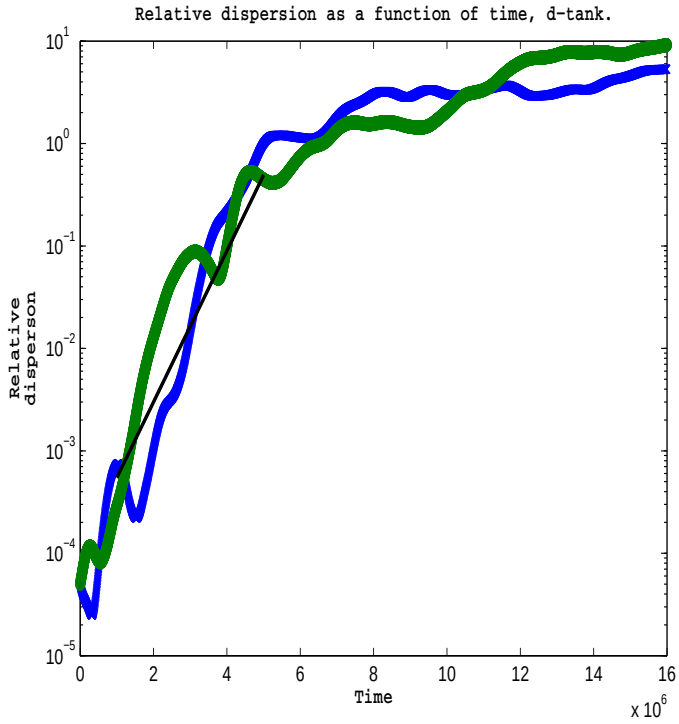

Figure 4.3: The relative dispersion for the zonal (x) and meridional (o) direction for the particles deployed in d-tank as a function of time. The straight line represents an exponential growth.

In Figure 4.4 the relative dispersion for the combined set (zonal + meridional) for the pairs as a function of time is plotted. The straight line again represents an exponential growth, and seem to be in better agreement with the relative dispersion in this plot. The relative dispersion and the exponential growth line fit up to time t = 5. Further growth does not proceed exponentially.

Again, the diffusivity normally gives a clearer result of the growth of the relative dispersion. Figure 4.5 shows the diffusivity for pairs of particles as a function of distance. The straight line now represents a dependency of scales squared ($K \propto D^2$), which corresponds to the k^{-3} energy spectrum, i.e. the enstrophy cascade range. For this measure, the growth is in very good agreement with the one predicted, thus the d-tank model data set is assumed to be within the enstrophy cascade range of the energy spectrum and to exhibit an exponetial growth for the relative dispersion.

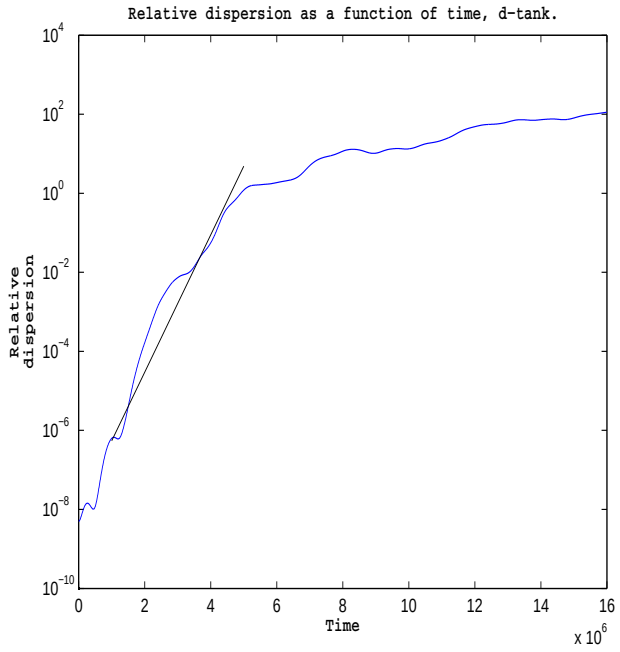

Figure 4.4: The relative dispersion for the zonal and meridional direction combined for the particles deployed in d-tank as a function of time. The straight line represents an exponential growth.

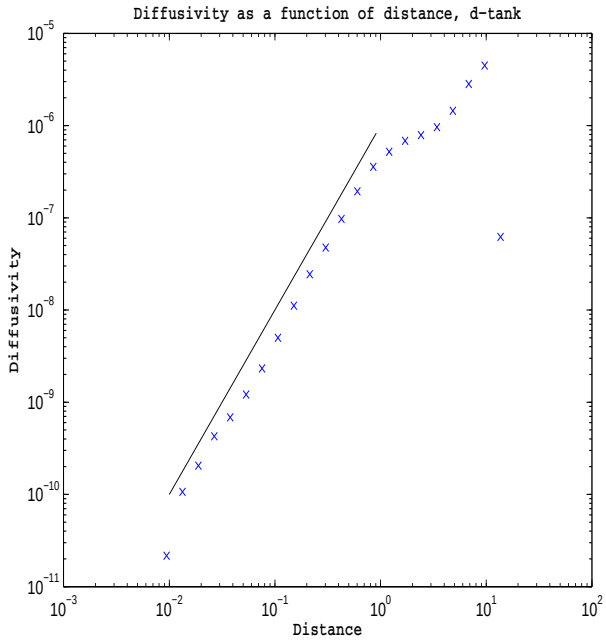

Figure 4.5: The diffusivity for d-tank data set as a function of distance. The straight line represents a distance squared growth, which corresponds to the k^{-3} energy spectrum.

4.2 SCULP data results

Compared to the majority of previous oceanic observation data sets, the SCULP data comprises much higher drifter densities, which implies more drifter pairs with close spacing, hence a better basis for statistical analyses at the smaller length scales (LaCasce and Ohlmann, 2003). The data used for this study are based on SCULP–I and -II deployments only as the data from SCULP–III is not suitable due to few drifter pairs and the specific problem this data were aimed at (section 3.2.1).

Figure 4.6 shows the relative dispersion for the combined SCULP–I and -II sets as a function of time. The straight line represents an exponential growth, thus implying that the underlying turbulence belongs in the enstrophy cascade range of the energy spectrum. After an initial adjustment of a day or so, the relative dispersion shows a good fit to this line for the first 10–11 days, according to length scales of 5-50 km. After day $\sim$ 11, the relative dispersion growth decreases and follows a power law growth. This power law growth for the latest times is shown in the loglog plot in Figure 4.7, where the straight line represents a power law growth of $t^{2.2}$ for the longest time scales.

SCULP data have formed the basis of several studies with highly various objectives, such as either a descriptive, statistical or dynamical focus. Ohlmann and Niiler (2005) examined the surface circulation in the northern Gulf of Mexico based on data from the SCULP drifters inter alia. LaCasce and Ohlmann (2003) studied the SCULP–I and -II data sets in regard to the relative motion of pairs and triplets of surface particles. The two particle statistics calculated in their study presented two growth phases: a nearly exponential growth up to 40–50 km separations, followed by a power law growth towards larger scales, i.e. in very good agreement with the results in this thesis. However, LaCasce and Ohlmann (2003) also calculated the finite–time, and the finite–scale Lyapunov exponents, (FTLE and FSLE, respectively), two measures highly suitable when the calculation in question (the relative dispersion) requires averaging. Figure 4.8 shows the FSLE for the full data set.

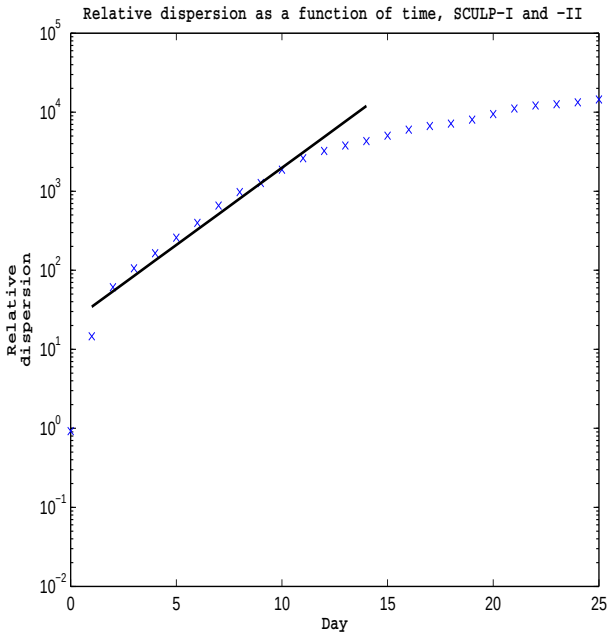

Figure 4.6: The relative dispersion for the combined SCULP-I and -II data sets as a function of time. The straight line represents an exponential growth.

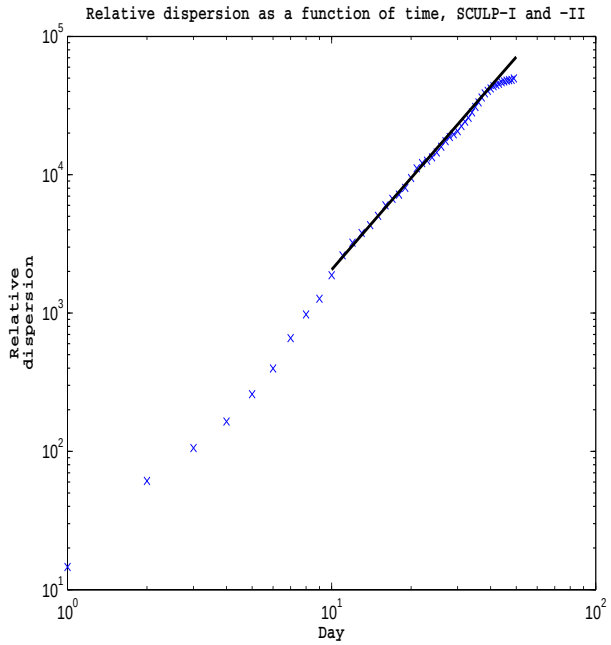

Figure 4.7: The relative dispersion for the combined SCULP-I and -II data sets as a function of time on a loglog plot. The straight line represents a power law growth.

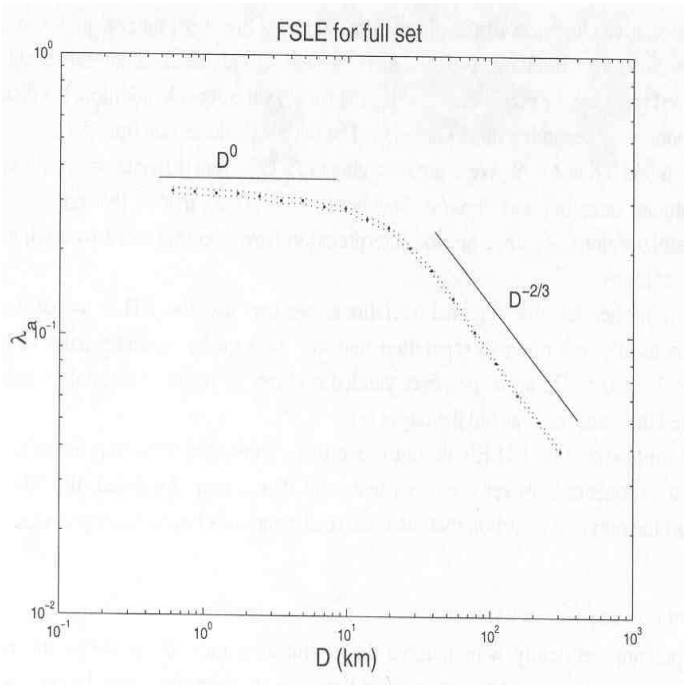

Figure 4.8: The FSLE for the full data set from the SCULP experiment. The dotted lines represents the 95% confidence limits, and the straight lines represent D^0 and $D^{\frac{-2}{3}}$ respectively. Figure from LaCasce and Ohlmann (2003), page 296.

Thus, the FSLE calculated by LaCasce and Ohlmann (2003) supported the exponential growth for the relative dispersion of pairs of particles at scales up to 40–50 km, which is in agreement with the results derived for the relative dispersion calculation by LaCasce and Ohlmann and the results in this thesis (Figure 4.6).

4.3 EOLE data results

Figure 4.9 shows the relative dispersion of the EOLE balloons as a function of time after launch. Only the first 10 days are shown in order to clarify the growth for the initial period, which is the period of greatest interest in this plot. The straigh line represents an exponential growth. However, it is difficult to determine exactly where the exponential growth line should be, as it can easily be constructed to fit any possible line that works as a tangent for the curve displayed by the dispersion growth for the first 3 days after launch. Nevertheless, further growth after day 3 decreases continuously.

Figure 4.10 shows the diffusivity of the EOLE balloons as a function of separation D. The two straight lines represent a D^2 (black line) and a $D^{\frac{4}{3}}$ (red line) power law, which correspond to an exponential and a power law growth, respectively. Again, as with the relative dispersion for the EOLE data, both lines can be a good fit, depending on where on the growth curve the tangent line is placed. It is also a slight possibility to match both the straight lines to the dispersion growth. The $D^{\frac{4}{3}}$ power law can be used for distances up to ~ 200 km, and then the D^2 power law is a better fit up to ~ 1000 km.

These difficulties in regard to firmly determining the dispersion growth for the initial period after launch are reflected in earlier studies based on the EOLE balloon data, e.g. the work by Morel and Larcheveque (1974) and Lacorata et al. (2004).

Morel and Larcheveque (1974) examined the EOLE data set and calculated the mean square relative velocity and mean diffusivity of balloon pairs separated by a distance D, trying to find the scale dependency of eddy diffusion on balloon pairs. In general, they established that the eddy dispersion process is homogeneous, isotropic and stationary up to scales of $D \sim 1000$ km. Figure 4.11 shows the root mean square separation of the original pairs of balloons from the EOLE experiment, as a function of time after launch. Morel and Larcheveque (1974) found that the mean separation of balloon pairs increased exponentially in time for the first 6 days, followed by a standard diffusion growth. Figure 4.12 shows the diffusivity for the EOLE balloon pairs as a function of distance. The straight line represents a power law of D^2, and Morel and Larcheveque (1974) concluded that the mean diffusivity has a scale dependency of D^2. Both the results of the mean square relative velocity and the mean diffusivity are compatible with the k^{-3} inertial range of the energy spectrum, for distances between 100–1000 km. These results are also in agreement with the work by Lin (1971), who concluded that the relative dispersion in the enstrophy-cascading inertial range (the k^{-3} range of the total kinetic energy spectrum) grows exponentially in time.

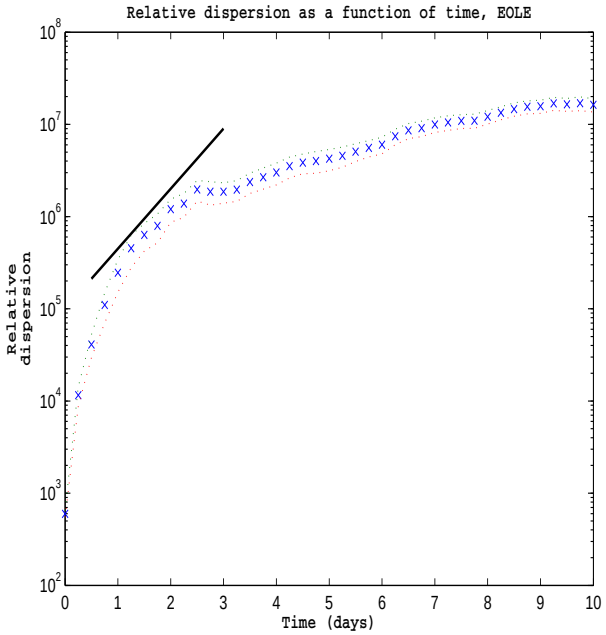

Figure 4.9: The relative dispersion for the EOLE balloons as a function of time after launch. The straight line represents a exponential growth. The dotted lines are the 95% confidence limits.

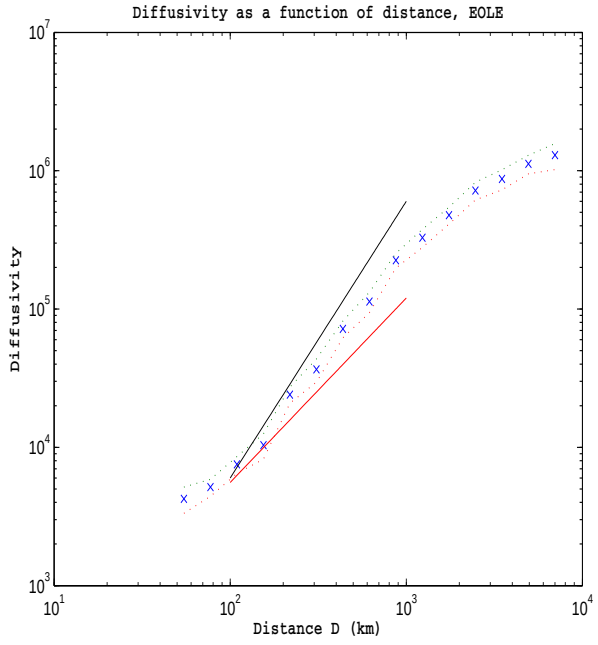

Figure 4.10: The diffusivity for the EOLE balloons as a funcion of distance. The straight black line represents a power law of D^2 while the straight red line represents a power law of $D^{\frac{4}{3}}$. The dotted lines are the 98% confidence limits.

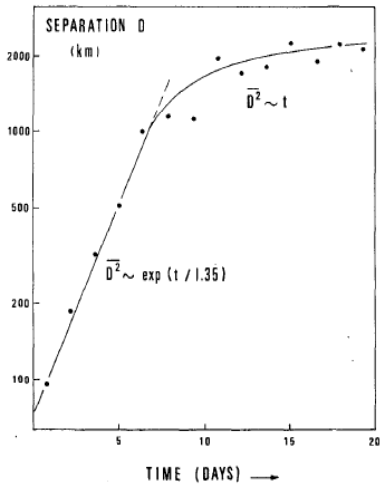

Figure 4.11: The mean squared relative vorticity for the EOLE balloons as a function of time after launch. The straight line represents an exponential growth. Figure from Morel and Larcheveque (1974), page 2194.

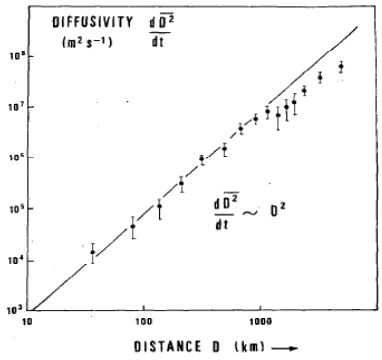

Figure 4.12: The mean square relative diffusivity of the EOLE balloon pairs as a function of distance. The straight line represents a D^2 law. Figure from Morel and Larcheveque (1974), page 2196.

However, Lacorata et al. (2004) revised the EOLE data set, and debated the conclusion made by Morel and Larcheveque (1974) for the growth of the relative dispersion. The reason for this revision was first of all a discrepancy between the conclusions made by Morel and Larcheveque (1974) and later studies based on aircraft data suggesting a $k^{\frac{-5}{3}}$ dependency range for the energy spectrum (i.e. Lindborg and Cho (2000)). In addition, the FSLE, a new tool for analyzing scale dependent properties, which was believed to improve the calculations, made this revision required. Lacorata et al. (2004) concluded that the initial dispersion indeed correspond to an exponential growth, and consequently to a k^{-3} dependency of the energy spectrum, but only for the first day after launch. The calculations of the further growth for day 2–6 instead showed a power law growth with the power gradually decreasing from 3 to 1, and therefore a $k^{\frac{-5}{3}}$ dependency of the energy spectrum.

The main result of this revision study was a $k^{\frac{-5}{3}}$ behaviour of the energy spectrum at inter-mediate scales of 100–1000 km, i.e. the opposite energy spectrum behaviour than stated by Morel and Larcheveque (1974). However, at distances smaller than 100 km, the results indicated an exponential growth, which is in slight agreement with the earlier studies. The reasons for the $k^{\frac{-5}{3}}$ spectrum were still not accounted for by, which yields the necessity for additional studies.

Chapter 5

Summary and conclusion

In this thesis, the relative dispersion of pairs of particles released in flows has been studied mainly with the use of two different statistical measures: the relative dispersion and the diffusivity.

The statistical measures of the relative dispersion are of major importance since the dispersal of a pollutant either in the ocean or atmosphere can be derived from this, both in regard to the mean drift and the spread. In addition, the relative dispersion is linked to the energy spectrum of the underlying flow, so in combining all these theories, important relations can be detected and used for e.g. predicting and controlling the dispersal of pollutants.

To form the basis for the statistical calculations, data from Lagrangian particle trajectories from two model data sets, one atmospheric observation data set and one ocean surface data set have been used. The model data were derived from a modified and simplified version of a numerical experiment model described in LaCasce and Brink (2000). Energy was added into the model in two distinct wavelength intervals, in an attempt to mirror the two different growth regimes of the relative dispersion corresponding to either the energy cascade range or the enstrophy cascade range of the underlying turbulence of the flow. The oceanic observation data set is a subset of the extensive data derived in the Surface CUrrent and Lagrangian Project (SCULP) conducted during the 1990s in the Gulf of Mexico (Ohlmann and Niiler, 2005). The atmospheric data set is a subset of the EOLE experiment which consisted of the launch of meteorological balloons at the 200 mb-level in the Southern Hemisphere during the 1980s (Morel and Bandeen, 1973).

The use of models are highly advantegeous in regard to collecting data, because as opposed to in situ observations, numerous particles can be deployed into the model and iterative runs can be executed so that the data set contains large numbers of particle pairs. The underlying dynamics that control the flow of the model is also known down to the smallest detail, resulting in a controlled experimental environment.

The pair statistics from experiments of forced, two-dimensional turbulent flows have therefore been examined, and compared with similar displacement distributions from oceanic and atmospheric observations.

In general, the calculations of the model data sets showed a good agreement with the expected developments of the relative dispersions. C-tank data set was forced in the interval $L = [\frac{2\pi}{60}, \frac{2\pi}{50}]$, which should result in the relative dispersion having a time dependency cubed and the diffusivity following Richardson's law, thus having a scale dependency of distance in the 4/3 power. The calculations of the c-tank data set presented both these results, hence the turbulence is within the energy cascade range of the energy spectrum, the $\kappa^{\frac{-5}{3}}$ range.

D-tank data set was forced in the interval $L = [\frac{2\pi}{5}, \frac{2\pi}{1}]$, and this should result in the relative dispersion following an exponential growth, and the diffusivity having a dependency of distance squared. The calculations of the d-tank data set presented both these results, hence the turbulence is within the enstrophy cascade range of the energy spectrum, the κ^{-3} range.

The results of the calculations of the SCULP data set showed, after an initial adjustment of one day, an exponential growth up to day ~ 11, according to length scales of 5–50 km, followed by a power law growth for the longest times. This is in good agreement with earlier studies of LaCasce and Ohlmann (2003).

The EOLE balloon data, however, showed rather indeterminable results. An exponential growth of any size could easily be made a tangent line to curve showing the relative dispersion for the initial period after launch. The diffusivity showed the same unsteadiness; both a power law of D^2 and a power law of $D^{\frac{-4}{3}}$ could be in agreement with the calculations. The difficulties of determining the relative dispersion, and consequently the energy spectrum for the EOLE data set, are still reflected among scientists, and the studies by (Morel and Larcheveque, 1974) and (Lacorata et al., 2004), concluded with an exponential growth and a power law growth respectively.

The difficulties in regard to determining the growth of the relative dispersion for some of the data sets used in this thesis can be due to the short interval in which a particle experiences the enstrophy cascade range of the energy spectrum. Note in Figure 4.5, that the distances for which the diffusivity and the straight line correspond, are in a the interval: $0.01 < \mathrm{D} < 1$. This implies that when particles enter the enstrophy cascade range, it is only a matter of time before a new regime, i.e. the energy cascade range, affects the turbulence, and consequently the dispersion of the particles. This means that the particles must adjust quickly when entering the enstrophy cascade range not to alter the statistics based on the flow within that particular range, by

being a statistical “outlier”.

The good agreements between predicted dispersion growths and the results presented by the model data calculations, implies that there is a need for iterative model experiments with different initial conditions, and/ or a slight altering of the energy interval in which the forcing is added. This will generate a larger data base, hence more thorough calculations that might make the knowledge of the different dispersal regimes clearer. Further studies with more extensive model data sets and comparisons between model experiments and observations from the atmosphere and ocean is therefore of great interest.

Bibliography

Davis, R.E. (1985) *D*rifter Observations of Coastal Surface Currents During CODE: The Method and Descriptive View. Journal of Geophysical Research, Vol. 90: p. 4741–4755.

Davis, R.E. (1991) *L*agrangian ocean studies. Annual Review of Fluid Mechanics, Vol. 23: p. 43–64.

Davis, R.E.; Webb, D.C.; Regier, L.A. and Dufour, J. (1992) *T*he Autonomous Lagrangian Circulation Explorer (ALACE). Journal of Atmospheric and Oceanic Technology, Vol. 9: p. 264–285.

Desbois, M. (1975) *L*arge-Scale Kinetic Energy Spectra from Eulerian Analysis of EOLE Wind Data. Journal of the Atmospheric Sciences, Vol. 32: p. 1838–1847.

Jullian, P.; Massman, W. and Levanon, N. (1977) *T*he TWERL Experiment. Bulletin of the American Meteorological Society, Vol. 58: p. 936–948.

LaCasce, J.H. (2008) *S*tatics of Lagrangian observations. Progress In Oceanography, Vol. 77: p. 1–29.

LaCasce, J.H. and Brink, K.H. (2000) *G*eostrophic Turbulence over a slope. Journal of Physical Oceanography, Vol. 30: p. 1305–1324.

LaCasce, J.H. and Ohlmann, C. (2003) *R*elative dispersion at the surface of the Gulf of Mexico. Journal of Marine Research, Vol. 61: p. 285–312.

Lacorata, G.; Aurell, E.; Legras, B. and Vulpiani, A. (2004) *E*vidence for a $k^{-}5/3$ Spectrum from the EOLE Lagrangian Balloons in the Low Stratosphere. Journal of the Atmospheric Sciences, Vol. 61: p. 2936–2942.

Lin, J.T. (1971) *R*elative Dispersion in the Enstrophy-Cascading Inertial Range of Homogeneous Two-Dimensional Turbulence. Journal of Atmospheric Science, Vol. 29: p. 394–396.

Lindborg, E. and Cho, J.Y.N. (2000) *D*etermining the Cascade of Passive Scalar Variance in the Lower Stratosphere. Physical Review Letters, Vol. 85: p. 5663–5666.

Morel, P. and Bandeen, W. (1973) *T*he Eole experiment: early results and current objectives. Bulletin American Meteorological Society, Vol. 54: p. 298–306.

Morel, P. and Desbois, M. (1974) *M*ean 200-mb Circulation in the Southern Hemisphere Deduced from EOLE Balloon Flights. Journal of the Atmospheric Sciences, Vol. 31: p. 394–407.

Morel, P. and Larcheveque, M. (1974) *R*elative Dispersion of Constant-Level Balloons in the 200-mb General Circulation. Journal of the Atmospheric Sciences, Vol. 31: p. 2189–2196.

Ohlmann, J. Carter and Niiler, P. Peter (2005) *C*irculation over the continental shelf in the northern Gulf of Mexico. Progress in Oceanography, Vol. 64: p. 45–81.

Richardson, L.F. (1926) *A*tmospheric Diffusion shown on a Distance-Neighbour Graph. Proceedings of the Royal Society of London, Vol. 110: p. 709–737.

Richardson, L.F. and Stommel, H. (1948) *N*ote on eddy diffusion in the sea. Journal of Meteorology, Vol. 5: p. 238–240.

Rossby, T.; Dorson, D. and Fontaine, J. (1986) *T*he RAFOS System. Journal of Atmospheric and Oceanic Technology, Vol. 3: p. 672–679.

Rossby, T. and Webb, D. (1970) *O*bserving abyssal motions by tracking Swallow floats in the SOFAR channel. Deep-Sea Research.

Stommel, H. and Arons, A.B. (1960) *O*n the abyssal circulation of the world ocean - II. An idealized model of the circulation pattern and amplitude in oceanic basins. Deep-Sea Research, Vol. 6.

Swallow, J.C. (1955) *A* neutral-buoyancy float for measuring deep currents. Deep-Sea Research, Vol. 3: p. 74–81.

Swallow, J.C. and Worthington, L.V. (1961) *A*n observation of a deep countercurrent in the western North Atlantic. Deep-Sea Research, Vol. 8: p. 1–19.

Taylor, G.I. (1915) *E*ddy motion in the atmosphere. Philosophical Transactions of the Royal Society of London, Vol. 215: p. 1–26.